Available online at www.sciencedirect.com
ScienceDirect
Trans. Nonferrous Met. Soc. China 32(2022) 2138−2149
Transactions of Nonferrous Metals Society of China
www.tnmsc.cn

Homogenization of twin-roll cast AA8079 aluminum alloy studied by in-situ TEM

R. KRÁLÍK, B. KŘIVSKÁ, L. BAJTOŠOVÁ, M. ŠLAPÁKOVÁ, M. CIESLAR

Faculty of Mathematics and Physics, Charles University, Ke Karlovu 3, 121 16 Prague 2, Czechia

Received 3 August 2021; accepted 6 April 2022

Abstract: AA8079 is a commonly used stock material for manufacturing thin packaging foils. The primary alloying elements Fe and Si can form binary and tertiary intermetallics. In-situ TEM simulating homogenization annealing process of the as-cast material was used to analyze the real-time changes of the shape, type, and distribution of these particles. They affect the mechanical properties of the final product and susceptibility of the material to the formation of pinholes and other macroscopic defects. Another set of as-cast samples were annealed in a regime simulating industrial treatment in combination with measurements of resistivity to validate the results of the in-situ experiment. The results show clear temperature intervals of recovery, matrix desaturation, and phase transformations occurring in several stages: spheroidization of the original particles above 450 °C, nucleation of new particles at 475 °C, particles coarsening above 525 °C, and an entire dissolution of the original particles above 550 °C.
Key words: aluminum alloys; in-situ annealing; homogenization; foil stock materials

1 Introduction

Aluminum is used as a stock material to manufacture thin packaging foils. It has good formability and corrosion resistance, and it is a good barrier for vapors and oxygen [1,2]. Aluminum foils can be easily coated, laminated, and printed, and all desired by the packaging industry. Aluminum is also highly recyclable. Fe and Si are primary alloying elements in the AA8xxx series of alloys including the AA8079 alloy [3]. Minimal attainable thicknesses are between 6 and 10 μm, depending on specific alloy compositions and selected processing methods [2].

During twin-roll casting (TRC), the alloy melt passes through a ceramic nozzle onto water-cooled rolls where the melt solidifies. The material is then subjected to a short period of hot rolling before leaving the water-cooled rolls entirely [4]. TRC can produce wide strips of the material several millimeters thick. This saves multiple rolling steps during downstream processing of thin foils compared to direct-chill (DC) casting that produces thicker ingots [2,4]. However, TRC suffers from various defects, including impurity inclusions, roll marks, surface bleeding of solute-rich melt, and so on [2,4−9]. Adjusting casting parameters diminishes most of these defects and will not be further discussed [7,8]. TRC strips also contain an inhomogeneous distribution of grains size, solutes, and dispersoid particles throughout the strip [4−7]. Deformation concentrates at these macroscopic inhomogeneities during cold rolling and often leads to poor mechanical properties of the final product. A homogenization annealing is performed at elevated temperatures to activate the diffusion of solute elements and grain boundary motion, eliminating some of the inhomogeneities. The intermetallic particles cannot be fully dissolved and

Corresponding author: R. KRÁLÍK, E-mail: rkralik96@gmail.com
DOI: 10.1016/S1003-6326(22)65936-3

are always present in the material due to the low solubility of Fe in Al [3]. The size and distribution of particles in the as-cast state and after homogenization affect processing behavior and final properties in several ways, including their effects on recrystallization [10].

Al_xFe and $Al_xFe_ySi_z$ phases are generally present in 8xxx series of aluminum alloys [3]. Particles in as-cast TRC materials form clusters along eutectic cells. The specific shape of the particles usually depends on their crystal structure, but there is a tendency towards the formation of fine and elongated particles in these systems [11−14]. The binary Al−Fe and ternary Al−Fe−Si systems are well described, and the equilibrium phases in the alloys are well known. In a low alloyed system, they are either the $Al_{13}Fe_4$ phase or the α-AlFeSi phase [15,16]. The former forms in systems with low Si content as Si is more soluble in Al than in Fe [14]. However, metastable phases can form due to the inherent non-equilibrium nature of TRC. These include phases from binary and ternary systems. Annealing at sufficiently elevated temperatures transforms these metastable phases into stable ones. Transformation of particles is one of the reasons why the homogenization step is performed at temperatures above 500 °C. This transformation typically incorporates redistribution of particles and their coarsening [17].

The present study provides information about high-temperature processes occurring during annealing using in-situ transmission electron microscopy (TEM), focusing on precipitation, dissolution, and growth of particles during homogenization, changes in particles morphology, and their distribution in the material. Real-time monitoring of these processes is possible through the in-situ annealing experiment in contrast with traditional methods of post-mortem analysis of conventionally annealed samples. The direct observations of otherwise well-described processes such as preferential positions of heterogeneous nucleation or Ostwald ripening [18] can be invaluable for understanding how a formation of microstructures observed in homogenized materials occurred. This information could be generalized for more accurate assessments in other similar materials. Although the in-situ annealing of a thin foil sample (generally used in TEM) is a powerful tool, it may not necessarily reflect the microstructural evolution of a real bulk sample due to a possibility of increased surface diffusion of solutes. Therefore, a post-mortem analysis of samples annealed in a regime simulating industrial annealing is required to validate these novel results. While as-cast and homogenized microstructures are well known and described, almost no research was done on the course of high-temperature microstructural changes occurring in the material. This information could play a crucial role in designing new technological processes resulting in a reduction of overall costs required by the energy-demanding homogenization.

2 Experimental

We studied a commercial twin-roll cast material. The studied AA8079 alloy contains 1.06 wt.% Fe and 0.06 wt.% Si. The concentration of alloying elements was determined by the Thermo Scientific ARL iSpark spectrometer by the provider of the material. The studied material has a relatively high Fe/Si molar ratio compared to other alloys of the same notation [14,17]. The supplied industrially cast strips of the material were 7 mm thick. The strips were cut using SiC cutting discs and further polished using a combination of mechanical and electrochemical polishing techniques.

The polished samples for light optical microscopy (LOM) were observed on a Zeiss Axio Observer 7 LOM using bright field and polarized light regimes. Sample preparation required chemical polishing in 0.5% HF in water solution (particles observations) and anodic oxidation at −15 °C in Barker's reagent (grain structure analysis). Samples for transmission electron microscopy were prepared by twin-jet electrolytic polishing in a 30% HNO_3 solution in methanol at −20 °C. Samples were analyzed on a JEOL JEM 2000FX TEM using bright field imaging and selected area electron diffraction (SAED) modes. The in-situ annealing was performed by TEM using a JEOL heating holder equipped with a Pt−PtRh thermo-couple for temperature control. The heating continued up to the thermal damage of the sample just below 600 °C. The effective heating rate was 5 °C/min with 25 °C steps. The crystallographic information of the identified phases originates from the PCD database [19]. The individual diffractograms were identified using CrystBox software [20].

Resistometry was performed on H-shaped samples using a four-point DC measurement in liquid nitrogen to monitor microstructural changes during isochronal annealing with steps of 20 °C/20 min. Each annealing step was finished by rapid quenching of the specimen into the water at room temperature. Post-mortem analyses of the quenched samples were performed on samples annealed in a simulated industrial annealing scheme. This scheme consists of 8 h linear heating, 8 h annealing at a requested temperature, and 8 h linear furnace cooling to room temperature.

3 Results

3.1 As-cast material

3.1.1 Light optical microscopy (LOM)

Intermetallic particles of primary phases in the as-cast material form colonies along eutectic cells (Fig. 1), which are elongated in the rolling direction due to applied forces during rolling. LOM observations have not revealed the centerline segregation [21].

The polarized light etching shows a grain structure (Fig. 2) typical for TRC materials [6]. Fine grains form in the surface layer of the strip due to an extremely high cooling rate due to direct contact of the molten alloy with water-cooled rolls. The rest of the strip comprises partially elongated grains with their longer axis inclined towards the rolling direction. The angle between the elongated grains and rolling direction, which is the largest in layers located near the surface, gradually decreases, reaching almost zero in the center of the strip. The grains have a higher aspect ratio closer to the surface of the strip, decreasing noticeably towards the center due to gradient cooling rates throughout the strip [22].

3.1.2 Transmission electron microscopy

TEM shows more details of the distribution of grains observed in LOM (Fig. 3). Higher magnification images confirm the formation of particle colonies by clusters of individual particles stacked parallel to each other into walls (Fig. 4). Scarce dislocations form cell walls or subgrain boundaries. Multiple diffractograms were taken on several intermetallic particles for identification of particles structure (Fig. 5(a)).

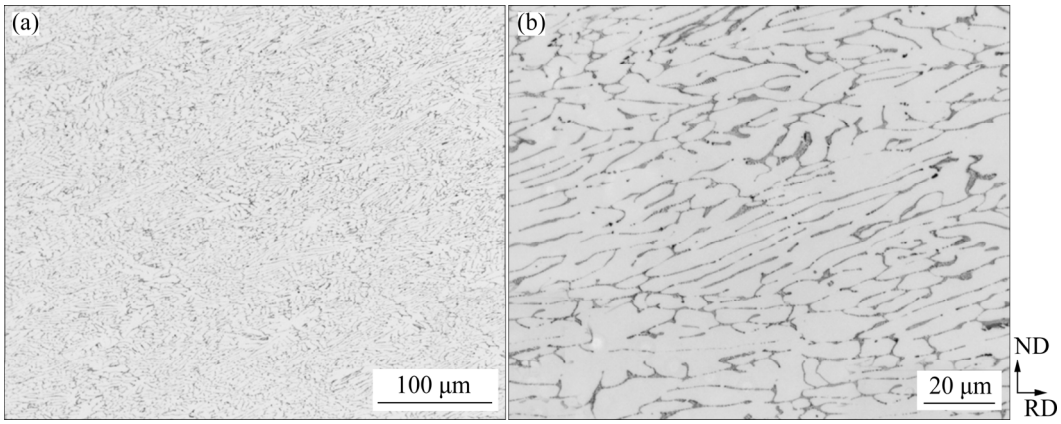

Fig. 1 Distribution of particles in as-cast AA8079 alloy in strip center at two different magnifications (ND and RD stand for normal and rolling directions, respectively)

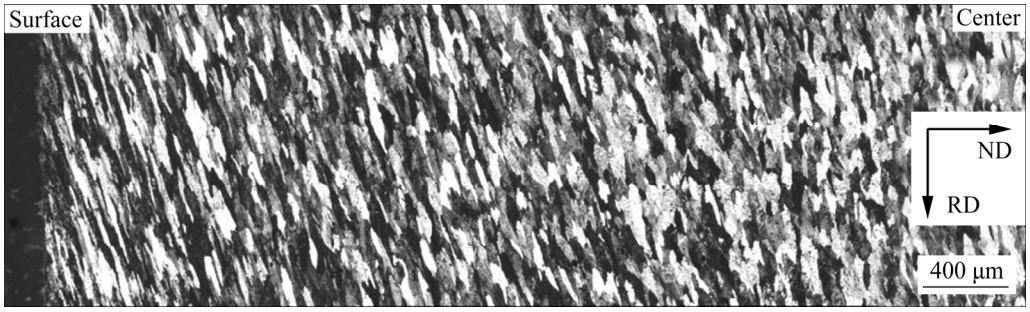

Fig. 2 Distribution of grains in as-cast AA8079 alloy (LOM image in polarized light)

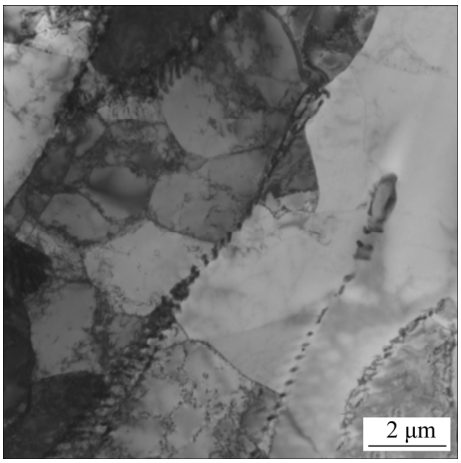

Fig. 3 TEM image of primary phase particles in eutectic cells and dislocation substructure in as-cast AA8079 alloy

We always identified the particles as hexagonal α-AlFeSi phase, also denoted as Al_8Fe_2Si [15] (Figs. 5(b, c)). Nevertheless, due to the selectivity of TEM, we cannot entirely exclude the presence of other particles of the Al−Fe−Si and Al−Fe systems.

3.2 Resistivity

Resistivity measurements can sensitively indicate temperature intervals associated with the solute redistribution through precipitation, dissolution, or polymorphic transformations of particles [23]. Resistivity linearly depends on the concentration of material defects in a first-order empirical approximation called Matthiessen's rule [24]. Deviations from this rule could indicate the presence of microstructural changes.

The resistivity curve (Fig. 6), obtained from a single isochronal measurement, shows only negligible variations below 300 °C, followed by a noticeable resistivity drop between 300 and 500 °C. Resistivity increases above this temperature interval. Local modifications of resistivity could be emphasized in the resistivity spectrum, i.e., a negative temperature derivative of the resistivity curve (Fig. 6). A significant spectrum feature is the presence of one pronounced peak, which is often observed in similar alloys [25,26] and could be correlated with a solid solution depletion [27].

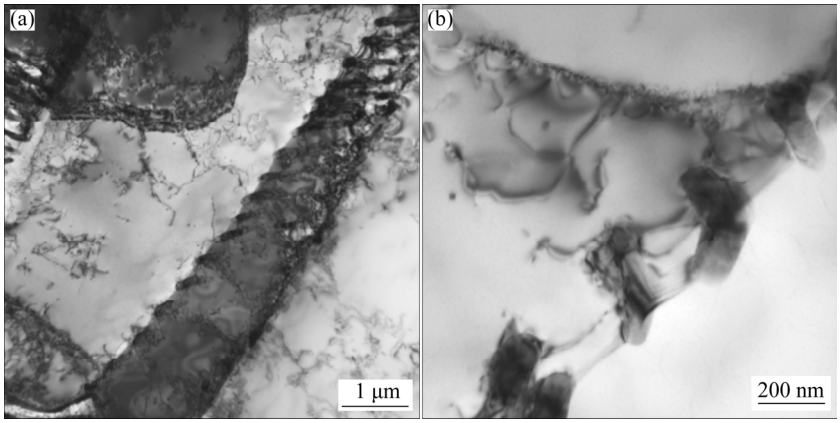

Fig. 4 TEM image of primary phase particle arrangement into cellular walls (a), and detailed image of individual particles (b) in as-cast AA8079 alloy

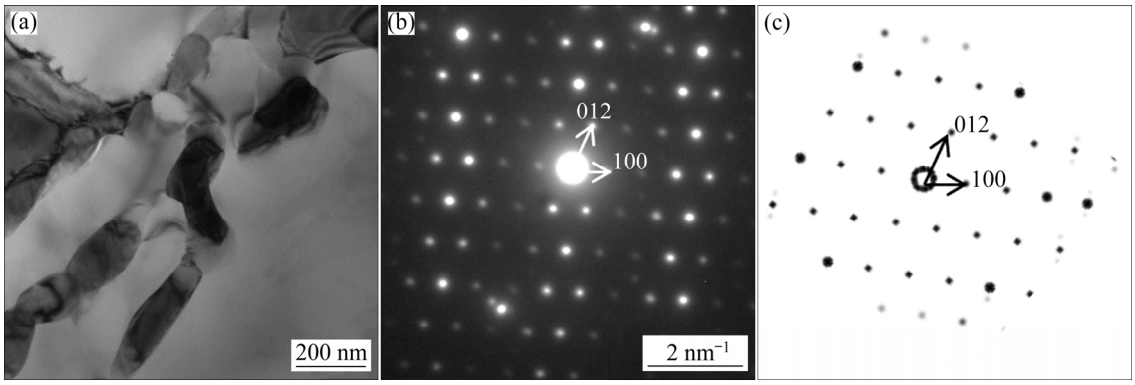

Fig. 5 Bright-field TEM image (a), SAED pattern from selected particle (marked by a circle) (b), and simulated electron diffraction of $[0\bar{2}1]$ zone of Al_8Fe_2Si phase (c)

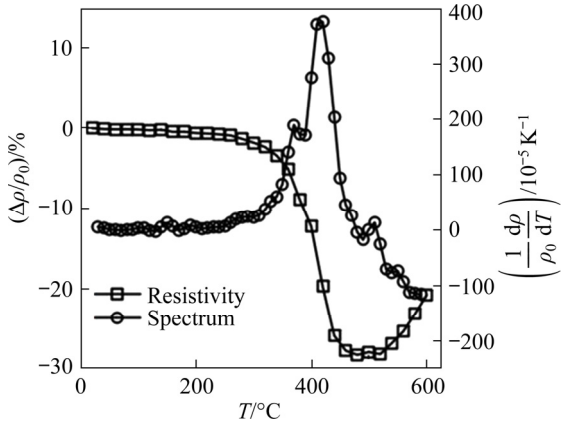

Fig. 6 Residual resistivity curve ($\Delta\rho/\rho_0-T$) and resistivity spectrum $\left(\frac{1}{\rho_0}\frac{\mathrm{d}\rho}{\mathrm{d}T}-T\right)$ of as-cast AA8079 alloy (ρ is the material resistivity, and $\Delta\rho$ is the resistivity change from initial resistivity ρ_0)

An increase of resistivity above 500 °C and corresponding negative values in the resistivity spectrum reflect the solid solution partial restoration. Individual resistivity values are measured with remarkably high precision (~0.01%). The experimental scatter of the relative change values is much lower than the size of the experimental point in Fig. 6.

3.3 TEM in-situ annealing

Figure 7(a) shows the as-cast state of an area selected for in-situ annealing observations containing colonies of primary phase particles and partially recovered substructure. The only microstructural changes occurring during annealing up to 325 °C (Fig. 7(b)) are the recovery of the dislocation substructure and the formation of well-defined subgrains.

No significant changes are observed up to 400 °C (Fig. 8(a)). First signs of partial dissolution and spheroidization of primary phase particles appear at 450 °C (Fig. 8(b)). Spheroidization is

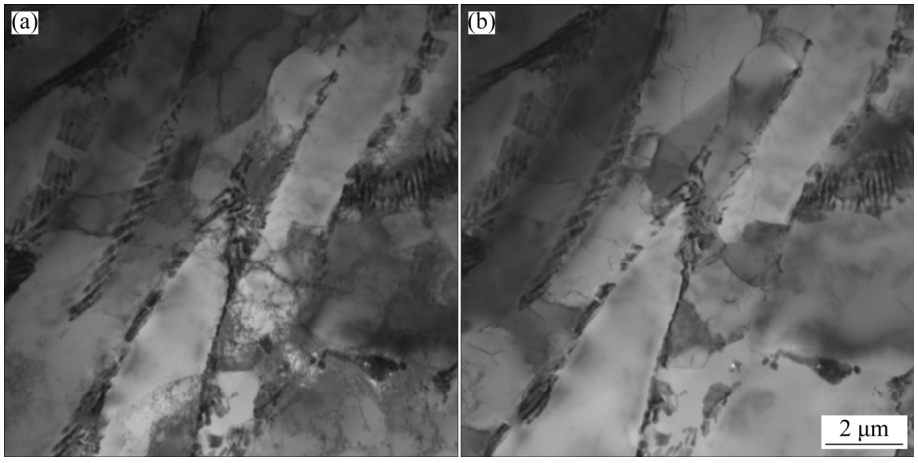

Fig. 7 TEM images showing overview of area selected for in-situ annealing in as-cast state (a), and recovered material after in-situ annealing at 325 °C (b)

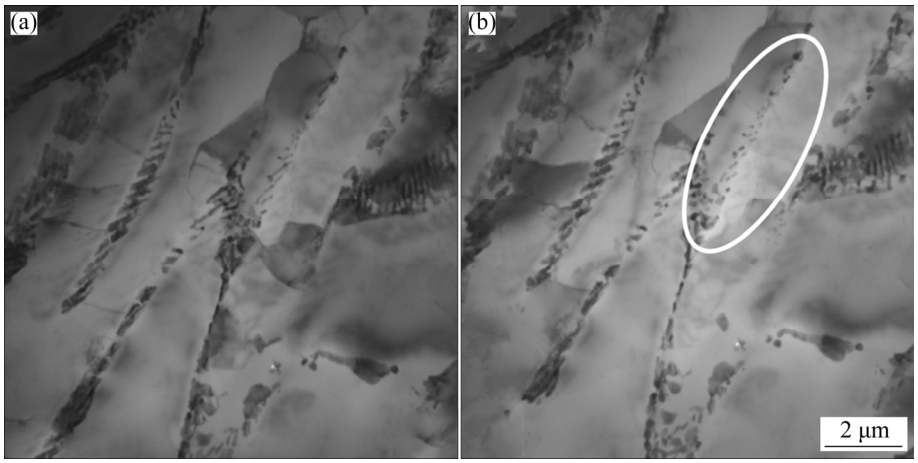

Fig. 8 Microstructure of AA8079 alloy after annealing up to 400 °C (stable structure) (a) and 450 °C (b) (first spheroidization marked by a white ellipse)

noticeable mainly in the highlighted area. The distribution of particles remains the same, and the overall change of particle morphology is minor.

The nucleation of new particles occurs at 475 °C inside original eutectic cells, which were previously particles-free (Fig. 9(a))). Spheroidization and partial dissolution of original particles proceed at 550 °C (Fig. 9(b)) and 550 °C (Fig. 9(c)). The dissolution accelerates at temperatures above 550 °C in favor of the growth of several coarser particles (Fig. 9(d)). Only a tiny fraction of the originally spheroidized particles remain at 575 °C (Fig. 10), and the material contains primarily coarser irregular particles.

According to recent observations [14] and our SAED analysis (Fig. 11) the annealed material should contain mainly $Al_{13}Fe_4$ phase due to a high Fe/Si molar ratio and a low overall content of alloying elements [16].

3.4 Post-mortem validation

The analysis of samples annealed in bulk conditions is necessary to validate results received during in-situ annealing. The microstructures of selected samples industrially annealed at 420, 460, 520, and 580 °C are shown in Fig. 12.

Similar to in-situ annealed specimens, no significant changes are observed in the bulk material annealed at 420 °C (Fig. 12(a)). A partial spheroidization of particles occurs at 460 °C (Fig. 12(b)), but the general shape of eutectic colonies remains unbroken. Most particles have a spherical shape at 520 °C (Fig. 12(c)) and there are also particles, which presumably nucleate during annealing, inside eutectic grains. The original primary phase particles dissolve at 580 °C (Fig. 12(d)) and the material contains mostly coarse particles of the $Al_{13}Fe_4$ phase.

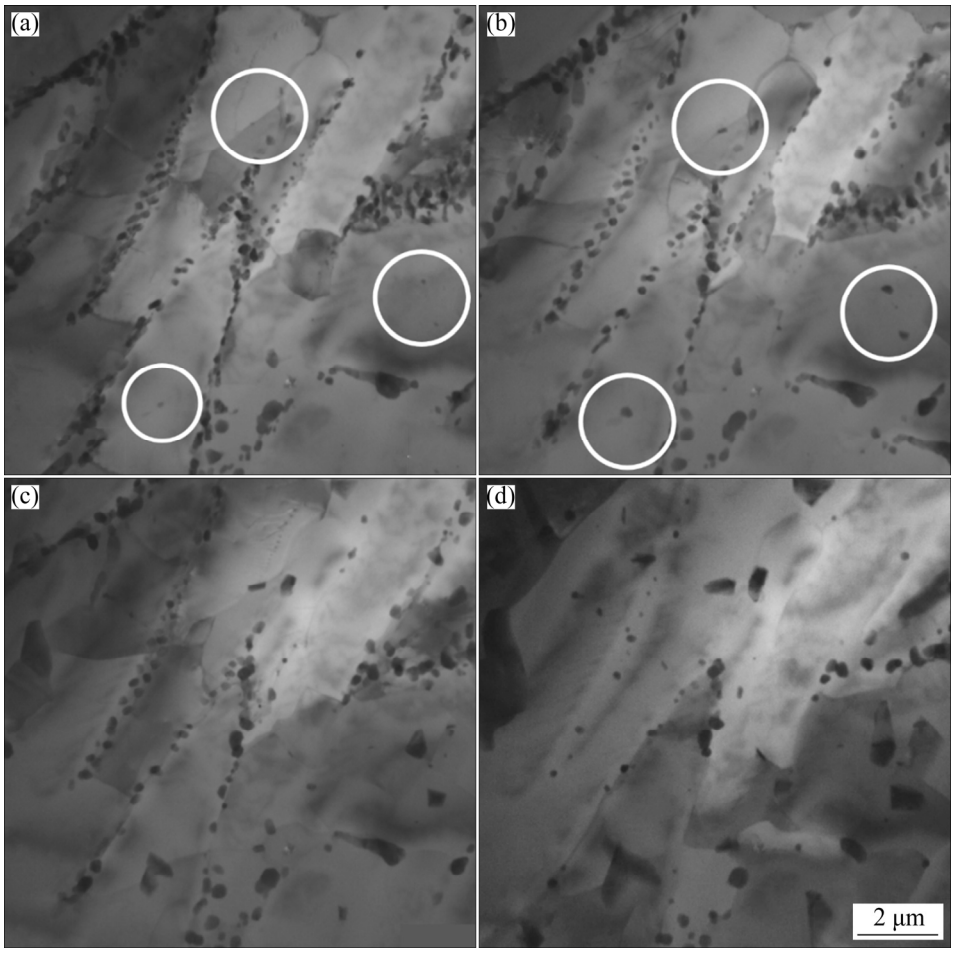

Fig. 9 TEM images showing microstructures during in-situ annealing of AA8079 alloy: (a) Nucleation of new particles (white circles) at subgrain boundaries at 475 °C; (b) Coarsening of new particles (white circles) at 525 °C; (c) Dissolution and coarsening of particles at 550 °C; (d) Acceleration of dissolution and coarsening at temperatures above 550 °C

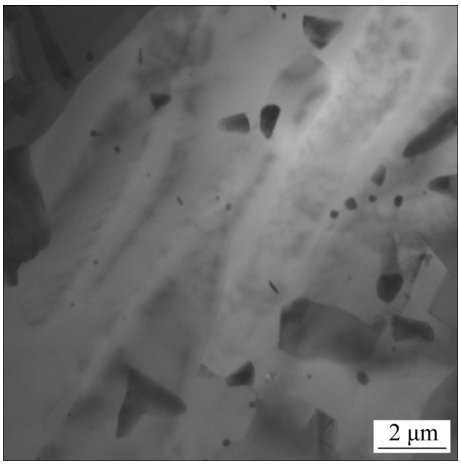

Fig. 10 TEM image of coarse particles in AA8079 alloy after in-situ annealing up to 575 °C

4 Discussion

Microstructural features observed in the AA8079 as-cast strip are generally detected in similar twin-roll cast aluminum alloys. A gradient grain structure and a dispersion of fine particles result from cooling rates and their gradient throughout the material during the casting process, regardless of the specific alloy composition and alloying elements [11,27−30]. A study made by SLÁMOVÁ et al [31] compares twin-roll cast and direct-chill cast (a more common method of aluminum alloys casting) structures. Due to lower cooling rates and different cooling gradients, direct-chill casting results in coarser grains and particles. While centerline segregation is a commonly observed defect in TRC materials in the AA8079 alloys and alloys of other systems [30,32], which was not observed in the present alloy. Lack of centerline segregation is probably a result of a proper setup of casting parameters combined with the casting of an alloy with a relatively low total content of alloying elements.

Several issues should be considered when resistivity and in-situ annealing are compared. A shallow decrease of resistivity below 300 °C reflects a slight dislocation density decrease in accordance with TEM observations. The dislocation density in the as-cast state is low due to a high temperature of hot working during casting. Therefore, recovery does not yield significant resistivity changes. On the other hand, almost no microstructural changes were observed in TEM close to 400 °C, but resistivity drops significantly in this temperature interval. Solute concentration, even at a low total percentage of solutes in the matrix, is a significant contributor to the total resistivity of the material ($25.6\times10^{-9}\,\Omega\cdot$m for 1 wt.% Fe [3], residual resistivity of Al in liquid nitrogen is ~$2.17\times10^{-9}\,\Omega\cdot$m [33]). The matrix is supersaturated due to the rapid cooling during casting. High temperatures activate the diffusion of these alloying elements from the matrix into intermetallic particles. These elements should either form new particles or cause an increase in their volume fraction. Nucleation of new particles was not observed in-situ in TEM at this stage. The initial concentration of Fe in the Al matrix was calculated, based on the measured resistivity, to be 0.05 at.%, while the total concentration in the alloy is 1.13 at.%. Diffusion of surplus Fe from the matrix into particles would lead to an approximately 5% increase of the volume ratio of Fe in matrix to Fe in particles, which shows a margin that TEM would barely notice. Annealing at higher temperatures results in a change of particle morphology and nucleation of new particles. The observed spheroidization of existing particles and limited

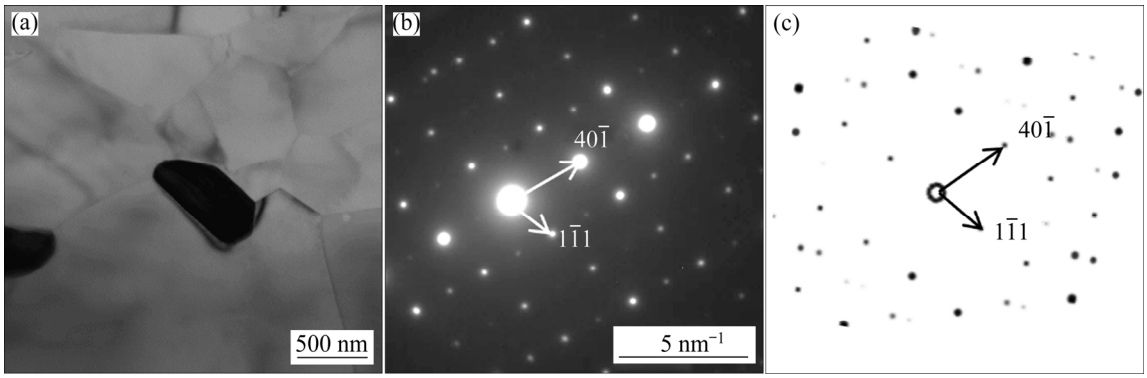

Fig. 11 TEM image of Fe-rich particle in bright field mode (a), SAED pattern of particle (b), and simulation of [154] zone of $Al_{13}Fe_4$ phase (c)

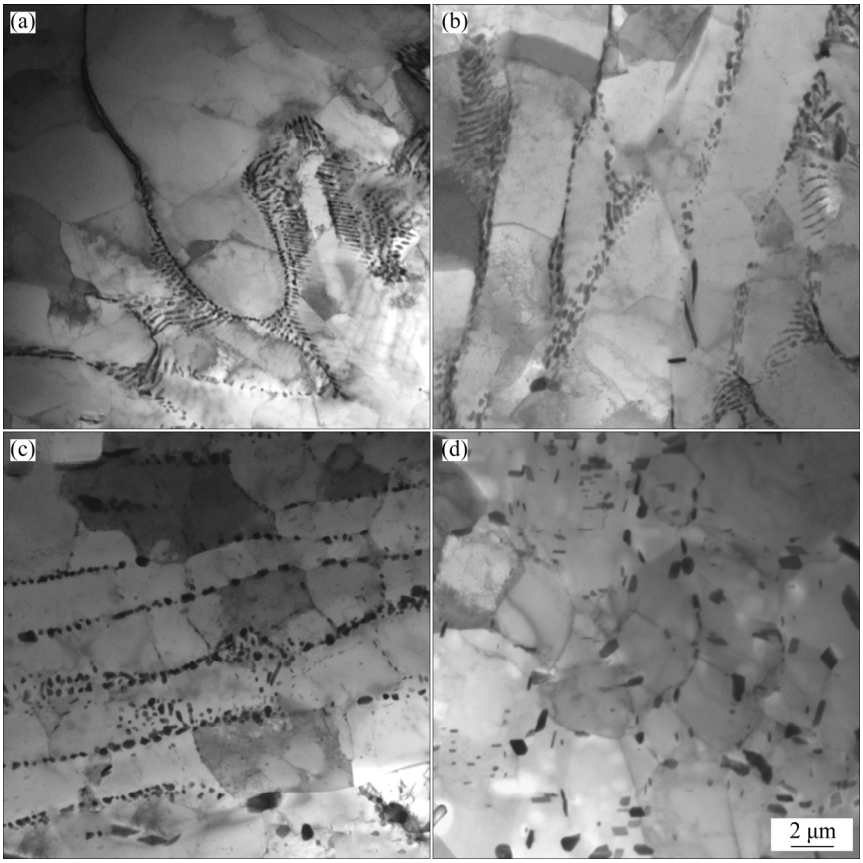

Fig. 12 Bright field TEM images of industrially annealed samples with almost no visible changes at 420 °C (a), spheroidization at 460 °C (b), additional spheroidization and nucleation of new particles at 520 °C (c), and microstructure at 580 °C containing mixture of transformed phases and newly formed particles (d)

nucleation affect resistivity only moderately because only limited depletion of the solid solution is expected at this phase. There is a steady increase of resistivity above 520 °C until the end of the selected annealing interval. This increase could be related to the redistribution of solutes between particles and the partial dissolution of existing particles. Several authors have observed similar resistivity behavior and confirmed that it is due to the reversion of the solid solution [14,34,35]. Especially the study made by LENTZ et al [14], including microprobe chemical analysis of the matrix, confirms the reversion of Fe back into the matrix at higher temperatures as the solubility limit of Fe in the matrix increases.

Though many metastable intermetallics can appear in AlFeSi based materials, the intermetallics present in the studied AA8079 alloy were mostly identified as α-AlFeSi and $Al_{13}Fe_4$ in the as-cast and finally annealed materials, respectively. Two notable studies using different identification methods, slightly different alloy compositions, and different casting methods were conducted by LENTZ et al [14] and BIROL [17]. BIROL [17] performed an XRD study on a twin-roll cast AA8079 alloy (6 mm in thickness with a higher Si content of 0.2 wt.% and 1 wt.% Fe. His study confirmed a continuous transformation of the α-AlFeSi phase into the equilibrium $Al_{13}Fe_4$ at higher annealing temperatures with an entire transformation finished at 600 °C. On the contrary, based on precise microprobe analyses, LENTZ et al [14] reported either the $Al_{13}Fe_4$ phase or other AlFe metastable phases in the as-cast state even in the alloy with a high Fe/Si molar ratio and a complete transformation into the equilibrium $Al_{13}Fe_4$ phase below 600 °C. The complete transformation process also includes an intermediate stage during which ternary intermetallics nucleate and redissolve. Their investigations on diluted 1xxx series alloys imply a required Si content higher than 0.1 wt.% necessary for forming ternary phases in the as-cast state [36]. Nevertheless, the apparent difference in the initial composition probably

originates from significantly lower solidification rates used in their study performed on direct-chill cast materials. Most probably, higher cooling rates in TRC alloys result in the formation of α-AlFeSi phase even at lower Si contents.

The XRD analysis of BIROL [17] implies a complete transformation of the α-AlFeSi phase into the stable $Al_{13}Fe_4$ phase. On the other hand, SHAKIBA et al [35], using EBSD identification, showed that the remaining undissolved spherical particles are still the α-AlFeSi phase. Their EBSD study was performed on a relatively diluted alloy with a lower Fe/Si molar ratio and the remaining particles dissolved below 600 °C leaving only the stable phase. Therefore, our results most probably do not contradict the results of BIROL [17] because the remaining spherical particles retaining the α-AlFeSi structure have a low volume fraction at high annealing temperatures and possibly could not be identified by XRD.

The requirement of electron transparency of TEM samples could increase the influence of surface diffusion in the thin sample and affect the results of in-situ experiments. However, comparison with post-mortem observations shows that the observed changes in a bulk material are in good agreement with the changes observed during the in-situ annealing. Several qualitative observations can therefore be reliably derived from the in-situ experiment. The spherical particles present in the material after homogenization at a lower temperature are formed by transforming the originally elongated particles present after casting. The original particles split into several smaller ones after a period of matrix depletion, and each of them then begins to spheroidize. Therefore, particle-free zones remain preserved inside original eutectic cells at lower annealing temperatures. Nucleation of new particles begins at higher annealing temperatures inside these particle-free zones. As shown in Fig. 9(a), particles nucleate on grain or subgrain boundaries, confirming preferential heterogeneous nucleation of particles during this annealing stage. Further coarsening of particles occurs at the expense of dissolution of the original spheroidized ones or their coagulation into a single coarser particle. The volume fraction of the original particles decreases gradually with increasing temperature. Some initially coarsened spheroidized particles could dissolve, unlike the newly formed ones, which remain stable even at the highest annealing temperatures, likely because they already have the structure of a stable $Al_{13}Fe_4$ phase immediately after nucleation. A schematic representation of the particle evolution is presented in Fig. 13.

In terms of the influence of the observed microstructures on other processing properties, both the coarse particles observed at 575 °C and the original eutectic colonies can potentially increase the likelihood of pinhole formation. Therefore, a compromise with a more homogeneous distribution of particles that have not yet coarsened seems optimal. This state could be reached because particles could nucleate in originally particle-free zones before any significant coarsening. However, more aspects of particles role must be kept in mind when designing the homogenization process. These include mechanisms of recrystallization control through intermetallic particles such as Zener drag and particle stimulated nucleation [30,31]. Particle stimulated nucleation is often used to produce a fine-grained material after rolling and a final recrystallization step. The process requires a homogeneous distribution of sufficiently large particles. This critical particle size depends on the amount of deformation stored in the material during rolling, but it is generally above 1 μm [10,37,38]. Therefore, our in-situ experiments could help to identify crucial temperatures and processes impacting the distribution and size of particles in the material, thus influencing the mechanism of controlling grain size and mechanical properties of a final foil.

5 Conclusions

(1) The as-cast state AA8079 aluminum alloy is typical for standard TRC structures. It contains colonies of fine particles formed around eutectic cells, both elongated in the rolling direction. The particles were identified as hexagonal α-AlFeSi phase.

(2) Dislocations originally organized in dislocation cells recover during the first stage of the annealing process below 325 °C. After this recovery, significant matrix depletion results in a decrease in the material's resistivity. This decrease lasts until 420 °C.

(3) Matrix depletion leads to a spheroidization

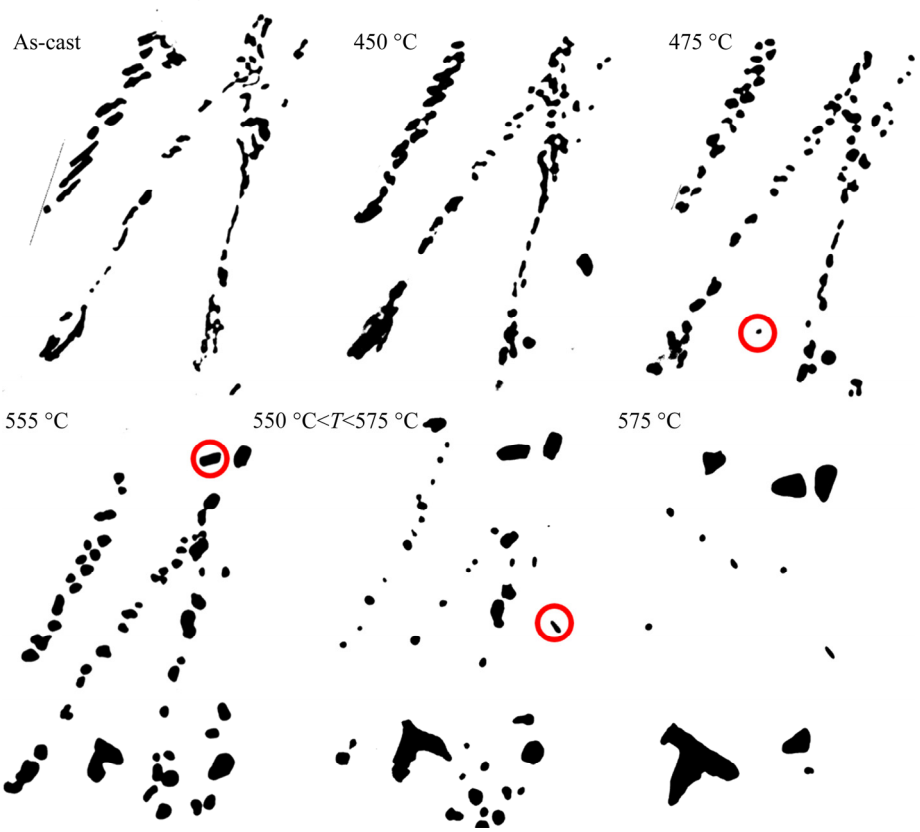

Fig. 13 Schematic representation of particle shape evolution during in-situ annealing (As-cast state—Elongated particles in colonies along eutectic cells at 450 °C—Initiation of spheroidization of particles at 475 °C—Continued spheroidization and nucleation of new particles (in red circles) at 550 °C—Dissolution and coarsening of selected particles at temperatures above 550 °C and below 575 °C—Continued coarsening and dissolution at 575 °C—Final structure containing mainly coarser particles)

of fine primary particles at 450 °C and nucleation of new particles. Several spheroidized particles and newly nucleated particles grow at the expense of most original ones up to 550 °C. Reversion of solute concentration then occurs, causing a monotonous increase of resistivity.

(4) Dissolution and growth of particles are accelerated above 550 °C. Only a tiny fraction of the original particles remain at 575 °C. The newly formed particles are much coarser and have been identified as the binary $Al_{13}Fe_4$ phase.

Acknowledgments

The financial supports of the Charles University Grant Agency Project (No. 704119) and Project TRIO FV (No. 20337) of the Czech Ministry of Industry and Trade are highly acknowledged.

References

[1] KERRY J. Packaging technology: Fundamentals, materials and processes (Chapter 9) [M]. Sawston: Woodhead Publishing Limited, 2012.

[2] KELES O, DUNDAR M. Aluminum foil: Its typical quality problems and their causes [J]. Journal of Materials Processing Technology, 2007, 186: 125−137.

[3] HATCH J E. Aluminum: Properties and physical metallurgy [M]. Metals Park, OH: American Society for Metals, 1984.

[4] COOK R, GROCOCK P G, THOMAS P M, EDMONDS D V, HUNT J D. Development of the twin-roll casting process [J]. Journal of Materials Processing Technology, 1995, 55: 76−84.

[5] YUN M, LOCKYER S A, HUNT J D. Twin roll casting of aluminium alloys [J]. Materials Science and Engineering A, 2000, 280: 116−123.

[6] GRAS C, MEREDITH M, HUNT J D. Microstructure and texture evolution after twin roll casting and subsequent cold rolling of Al−Mg−Mn aluminium alloys [J]. Journal of Materials Processing Technology, 2005, 169: 156−163.

[7] LOCKYER S A, YUN M, HUNT J D, EDMONDS D V. Micro- and macrodefects in thin sheet twin-roll cast aluminum alloys [J]. Materials Characterization, 1996, 37: 301−310.

[8] LEE Y S, KIM H W, CHO J H. Effect of casting parameters on roll separation force during twin-roll casting [J]. Procedia Engineering, 2014, 81: 1547−1552.

[9] SONG R, HARADA Y, KUMAI S. Twin roll casting of aluminum alloy strips [J]. Journal of Materials Processing Technology, 2017, 153/154**:** 42−47.

[10] HUMPHREYS F J, HATHERLY M. Recrystallization and related annealing phenomena [M]. 2nd ed. Amsterdam: Elsevier, 2004.

[11] BIROL Y. Analysis of macro segregation in twin-roll cast aluminium strips via solidification curves [J]. Journal of Alloys and Compounds, 2009, 468: 168−172.

[12] SPATHIS D, TSIROR J. The influence of casting speed in the as-cast strip mechanical properties of 8079 and 8006 alloys [C]//Light Metals 2013. Heidelberg: Springer, 2016: 305−309.

[13] ENGLER O, AEGERTER J, CALMER D. Control of texture and earing in aluminium alloy AA8011A-H14 closure stock [J]. Materials Science and Engineering A, 2020, 775: 138965.

[14] LENTZ M, LAPTYEVA G, ENGLER O. Characterization of second-phase particles in two aluminium alloy foil alloys [J]. Journal of Alloys and Compounds, 2016, 660: 276−288.

[15] ROGER J, BOSSELET F, VIALA J C. X-rays structural analysis and thermal stability studies of the ternary compound α-AlFeSi [J]. Journal of Solid State Chemistry, 2011, 184: 1120−1128.

[16] BLACK P J. The structure of $FeAl_3$ [J]. Acta Crystallographica, 1955, 8: 175−182.

[17] BIROL Y. Thermomechanical processing of a twin-roll cast Al−1Fe−0.2Si alloy [J]. Journal of Materials Processing Technology, 2008, 202: 564−568.

[18] TOKUYAMA M, KAWASAKI K, ENOMOTO Y. Kinetic equations for Ostwald ripening [J]. Physica A: Statistical Mechanics and its Applications, 1986, 134: 323−338.

[19] BRANDENBURG K, PUTZ H, BERNDT M. Pearson's crystal data [EB/OL]. 2021−08−03. http://www.crystal-impact.com/pcd/.

[20] MIROSLAV K. Crystbox software [EB/OL]. 2021−08−03. https:// www.fzu.cz/~klinger/crystbox.pdf.

[21] JIN I, MORRIS L R, HUNT J D. Centerline segregation in twin-roll-cast aluminum alloy slab [J]. JOM Science, 1982, 34: 70−75.

[22] SUN N, PATTERSON B R, SUNI J P. Microstructural evolution in twin roll cast AA3105 during homogenization [J]. Materials Science and Engineering A, 2006, 416: 232−239.

[23] HÁJEK M, VESELÝ J, CIESLAR M. Precision of electrical resistivity measurements [J]. Materials Science and Engineering A, 2007, 462: 339−342.

[24] KITTEL C. Introduction to solid state physics [M]. 8th ed. Hoboken, NJ: Wiley, 2005.

[25] POKOVÁ M, CIESLAR M, LACAZE J. The influence of silicon content on recrystallization of twin-roll cast aluminum alloys for heat exchangers [J]. Acta Physica Polonica A, 2012, 122: 625−629.

[26] CIESLAR M, SLAMOVA M, UHLIR J, COUPEAU C H, BONNEVILLE J. Effect of composition and work hardening on solid solutiondecomposition in twin-roll cast Al−Mn sheets [J]. Kovove Materialy, 2007, 45: 91−98.

[27] EIVANI A R, AHMED H, ZHOU J, DUSZCZYK J. Correlation between electrical resistivity, particle dissolution, precipitation of dispersoids, and recrystallization behavior of AA7020 aluminum alloy [J]. Metallurgical and Materials Transactions A, 2009, 40: 2435−2446.

[28] BIROL Y. Homogenization of a twin-roll cast thin Al−Mn strip [J]. Journal of Alloys and Compounds, 2009, 471: 122−127.

[29] BAREKAR N S, DHINDAW B K. Twin-roll casting of aluminum alloys — An overview [J]. Materials and Manufacturing Processes, 2014, 29: 651−661.

[30] MALCIOGLU A U, DOGAN C, INEL C, GODE C. Effects of casting speed on thin gauge foil surface quality of 8079 aluminum alloy produced by twin roll casting method [J]. Transactions of the Indian Institute of Metals, 2019, 72: 1001−1011.

[31] SLÁMOVÁ M, KARLÍK M, ROBAUT F, SLÁMA P, VÉRON M. Differences in microstructure and texture of Al−Mg sheets produced by twin-roll continuous casting and by direct-chill casting [J]. Materials Characterization, 2002, 49: 231−240.

[32] GRYDIN O, STOLBCHENKO M, SCHAPER M, BELEJOVÁ S, KRÁLIK R, BAJTOŠOVA L, KŘIVSKÁ B, HÁJEK M, CIESLAR M. New twin-roll cast Al−Li based alloys for high-strength applications [J]. Metals, 2020, 10: 987−1002.

[33] DESAI P D, JAMES H M, HO C Y. Electrical resistivity of aluminum and manganese [J]. Journal of Physical and Chemical Reference Data, 1984, 13: 1131−1172.

[34] TILAK R V, MORRIS J G. Studies of the effect of thermomechanical treatments on the supersaturation content of strip-cast aluminum alloy 3004 [J]. Materials Science and Engineering, 1985, 73: 139−150.

[35] SHAKIBA M, PARSON N, CHEN X G. Effect of homogenization treatment and silicon content on the microstructure and hot workability of dilute Al−Fe−Si alloys [J]. Materials Science and Engineering A, 2014, 619: 180−189.

[36] ALLEN C M, O'REILLY K A Q, CANTOR B, EVANS P V. Intermetallic phase selection in 1xxx Al alloys [J]. Progress in Materials Science, 1998, 43: 89−170.

[37] HUMPHREYS F J. The nucleation of recrystallization at second phase particles in deformed aluminium [J]. Acta Metallurgica, 1977, 25: 1323−1344.

[38] NES E, RYUM N, HUNDERI O. On the Zener drag [J]. Acta Metallurgica, 1985, 33: 11−22.

原位透射电镜研究双辊铸造 AA8079 铝合金的均匀化过程

R. KRÁLÍK, B. KŘIVSKÁ, L. BAJTOŠOVÁ, M. ŠLAPÁKOVÁ, M. CIESLAR

Faculty of Mathematics and Physics, Charles University, Ke Karlovu 3, 121 16 Prague 2, Czechia

摘　要：AA8079 铝合金是一种常用的制造薄包装箔的胚料，其主要的合金化元素 Fe 和 Si 可以形成二元和三元金属间化合物。采用原位透射电镜模拟铸态材料均匀化退火，分析这些颗粒的形状、类型和分布的实时变化，它们影响最终产品的力学性能、材料对形成气孔和其他宏观缺陷的敏感性。对另一组铸态样品在模拟工业热处理制度范围内进行退火处理，并结合电阻率测量，验证原位试验的结果。结果表明，在 450 ℃以上的原始颗粒球化、475 ℃的新颗粒成核、525 ℃以上的颗粒粗化以及 550 ℃以上的原始颗粒完全溶解等几个阶段发生了回复、基体去饱和以及相变，且具有明显的温度区间。

关键词：铝合金；原位退火；均匀化；箔胚料

(Edited by Wei-ping CHEN)